



Microscopic mechanism of high-temperature ferromagnetism in Fe, Mn, and Cr-doped InSb, InAs, and GaSb magnetic semiconductors

Jing-Yang You ¹, Bo Gu ^{1,2,*}, Sadamichi Maekawa,^{3,1} and Gang Su^{1,2,4,†}

¹*Kavli Institute for Theoretical Sciences, and CAS Center for Excellence in Topological Quantum Computation, University of Chinese Academy of Sciences, Beijing 100190, China*

²*Physical Science Laboratory, Huairou National Comprehensive Science Center, Beijing 101400, China*

³*Center for Emergent Matter Science, RIKEN, Wako 351-0198, Japan*

⁴*School of Physical Sciences, University of Chinese Academy of Sciences, Beijing 100049, China*



(Received 12 July 2020; revised 7 September 2020; accepted 10 September 2020; published 24 September 2020)

In recent experiments, high Curie temperatures T_c above room temperature were reported in ferromagnetic semiconductors Fe-doped GaSb and InSb, while low T_c between 20 K to 90 K were observed in some other semiconductors with the same crystal structure, including Fe-doped InAs and Mn-doped GaSb, InSb, and InAs. Here we study systematically the origin of high temperature ferromagnetism in Fe, Mn, Cr-doped GaSb, InSb, and InAs magnetic semiconductors by combining the methods of density functional theory and quantum Monte Carlo. In the diluted impurity limit, the calculations show that the impurities Fe, Mn, and Cr have similar magnetic correlations in the same semiconductors. Our results suggest that high (low) T_c obtained in these experiments mainly comes from high (low) impurity concentrations. In addition, our calculations predict the ferromagnetic semiconductors of Cr-doped InSb, InAs, and GaSb that may have possibly high T_c . Our results show that the origin of high T_c in (Ga,Fe)Sb and (In,Fe)Sb is not due to the carrier induced mechanism because Fe^{3+} does not introduce carriers.

DOI: [10.1103/PhysRevB.102.094432](https://doi.org/10.1103/PhysRevB.102.094432)

I. INTRODUCTION

Magnetic semiconductors, which combine the dual characteristics of ferromagnets and semiconductors, are basic materials for next-generation semiconductor devices. Practical applications require that magnetic semiconductors can work at room temperature, which is a big challenge in science [1]. Over the past three decades, magnetic semiconductor studies were focused on the diluted magnetic semiconductors. The representative material is Mn-doped p -type semiconductors (Ga,Mn)As [2], in which the highest Curie temperature T_c is currently about 200 K [3]. How to increase T_c in (Ga,Mn)As has become a hot topic under intensive exploration [4]. In order to avoid various difficulties caused by valence state mismatch in magnetic doping in (Ga,Mn)As, great progress has been made in the diluted magnetic semiconductors with independently adjustable magnetic moments and carriers concentrations. In 2007, a theoretical study predicted the ferromagnetic semiconductor Li(Zn,Mn)As with decoupled magnetic moments and carriers doping [5]. In 2011, the experiment obtained the Mn-doped p -type ferromagnetic semiconductor Li(Zn, Mn)As with T_c of 50 K [6]. In the same ferromagnetic semiconductor family, experiments realized Mn-doped p -type Li(Zn,Mn)P with T_c of 34 K [6] and Li(Cd,Mn)P with T_c of 45 K [7]. In 2013, the experiment discovered Mn-doped p -type ferromagnetic semiconductor (Ba, K)(Zn, Mn)₂As₂ with a higher T_c of

230 K [8,9]. Motivated by the experimental high T_c , the density functional theory calculation [10] and photoemission spectroscopy experiments [11,12] were conducted to understand the microscopic mechanism of ferromagnetism in (Ba, K)(Zn, Mn)₂As₂. Since 2016, the T_c higher than room temperature has been reported in the experiments of Fe-doped p -type ferromagnetic semiconductor (Ga,Fe)Sb [13–16].

In addition to the p -type diluted ferromagnetic semiconductors, studies on the n -type diluted ferromagnetic semiconductors have also made great progress. In 2016, a theory proposed a physical picture of the diluted ferromagnetic semiconductors with narrow band gaps, which can form ferromagnetism controlled by n -type and p -type carriers, while diluted ferromagnetic semiconductors with wide band gaps can only form ferromagnetism controlled by p -type carriers [17–19]. In 2017, the experiment reported the T_c higher than room temperature in Fe-doped n -type ferromagnetic semiconductor (In,Fe)Sb [20], and later the experiment found that a gate voltage in (In,Fe)Sb can turn its T_c [21,22]. The origin of high T_c in (In,Fe)Sb and (Ga,Fe)Sb has been discussed based on the density functional theory calculation [23]. In 2019, the experiment obtained a T_c of 45 K in Co-doped n -type semiconductor Ba(Zn, Co)₂As₂ [24].

In contrast to the high T_c above room temperature obtained in Fe-doped p -type (Ga,Fe)Sb and n -type (In,Fe)Sb, low Curie temperatures of 25 K and 10 K were obtained in the experiments of Mn-doped p -type (Ga,Mn)Sb [25] and p -type (In,Mn)Sb [26], respectively. In addition, T_c of 70 K was obtained in Fe-doped n -type (In,Fe)As [27,28], and 90 K was obtained in the Mn-doped p -type (In,Mn)As [29].

*gubo@ucas.ac.cn

†gsu@ucas.ac.cn

Ferromagnetic semiconductors have intriguing applications both in their own right and in guiding materials advances in other systems, such as spin-orbit torque and spin-polarized current-induced creep [30]. In addition, both p and n -doped high-temperature ferromagnetic semiconductors may offer opportunities that are not available in high-temperature ferromagnetic metals. One could design various bipolar devices, including transistors for spin-controlled amplification [31].

In order to understand the microscopic mechanism of high T_c in Fe-doped GaSb and InSb, and low T_c in Fe-doped InAs and Mn-doped GaSb, InSb and InAs, in this paper we carry out a systematic theoretical study based on the combined method of density functional theory and quantum Monte Carlo. In the diluted impurity limit, our calculations show that the impurities Fe, Mn, and Cr have similar magnetic correlations in the same semiconductors. Thus, we argue that high (low) T_c in these experiments mainly comes from high (low) impurity concentrations. Our calculations predict ferromagnetic semiconductors Cr-doped InSb, InAs, and GaSb that may have high T_c . Our results show that the origin of high T_c in (Ga,Fe)Sb and (In,Fe)Sb is not due to the carrier induced mechanism because Fe^{3+} does not introduce carriers. Thus, in order to increase T_c in diluted ferromagnetic semiconductors, a primary strategy is to increase the impurity concentrations while keeping the crystal structures unchanged, for example by choosing proper impurities and host semiconductors to avoid valence state mismatch during host doping.

II. DFT+QMC METHOD

We use a combination of the density functional theory (DFT) [32,33] and the Hirsch-Fye quantum Monte Carlo (QMC) simulation [34]. Our combined DFT+QMC method can be used for an in-depth treatment of band structures of host materials and strong electron correlations of magnetic impurities on equal footing. It can be applied for designing functional semiconductor- [35–37] and metal-based [38–40] materials. The method involves two calculations steps. First, with the Anderson impurity model [41], the host band structure and impurity-host mixing are calculated using the DFT method. Second, magnetic correlations based on the Anderson impurity model at finite temperatures are calculated using Hirsch-Fye QMC technique [34]. Considering the cost of calculation and the accuracy of the results, we set the temperature at 360 K.

The Anderson impurity model is defined as follows:

$$\begin{aligned}
 H = & \sum_{\mathbf{k}, \alpha, \sigma} [\epsilon_{\alpha}(\mathbf{k}) - \mu] c_{\mathbf{k}\alpha\sigma}^{\dagger} c_{\mathbf{k}\alpha\sigma} + \sum_{\mathbf{k}, \alpha, \mathbf{i}, \xi, \sigma} (V_{\mathbf{i}\xi\mathbf{k}\alpha} d_{\mathbf{i}\xi\sigma}^{\dagger} c_{\mathbf{k}\alpha\sigma} \\
 & + \text{H.c.}) + (\epsilon_d - \mu) \sum_{\mathbf{i}, \xi, \sigma} d_{\mathbf{i}\xi\sigma}^{\dagger} d_{\mathbf{i}\xi\sigma} + U \sum_{\mathbf{i}, \xi} n_{\mathbf{i}\xi\uparrow} n_{\mathbf{i}\xi\downarrow},
 \end{aligned} \quad (1)$$

where $c_{\mathbf{k}\alpha\sigma}^{\dagger}$ ($c_{\mathbf{k}\alpha\sigma}$) is the creation (annihilation) operator for a host electron with wave vector \mathbf{k} and spin σ in the valence bands ($\alpha = v$) or conduction bands ($\alpha = c$), and $d_{\mathbf{i}\xi\sigma}^{\dagger}$ ($d_{\mathbf{i}\xi\sigma}$) is the creation (annihilation) operator for a localized electron at impurity site \mathbf{i} in orbital ξ and spin σ with $n_{\mathbf{i}\xi\sigma} = d_{\mathbf{i}\xi\sigma}^{\dagger} d_{\mathbf{i}\xi\sigma}$. Here, $\epsilon_{\alpha}(\mathbf{k})$ is the band structure of host semiconductor, μ

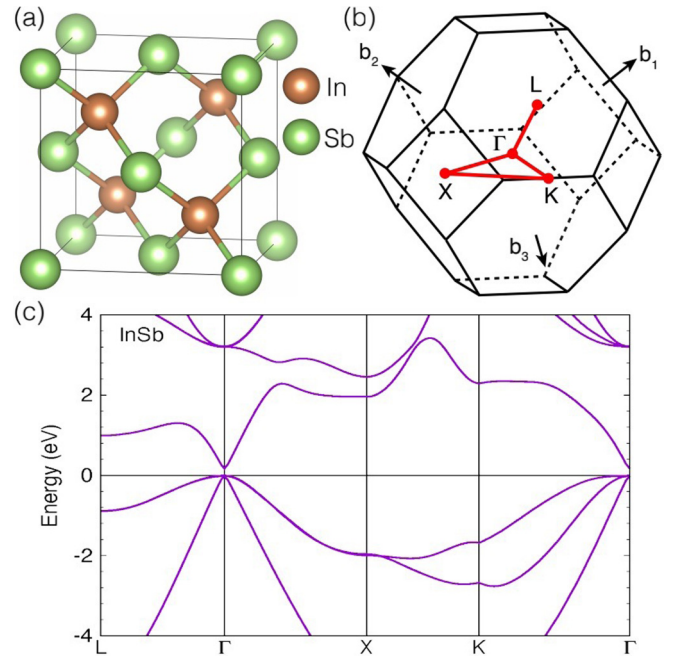


FIG. 1. (a) The crystal structure of InSb and (b) its first Brillouin zone with high symmetry paths indicated. (c) Energy bands ϵ_{α} of host semiconductor InSb. A direct band gap of 0.17 eV was obtained by DFT calculations with the modified Becke-Johnson (mBJ) exchange potential, which agrees well with the experimental value.

is the chemical potential, $V_{\mathbf{i}\xi\mathbf{k}\alpha}$ denotes the mixing parameter between impurity and host electrons, ϵ_d is the impurity $3d$ orbital energy, and U is the onsite Coulomb repulsion of the impurity. Considering the condition of Hund coupling $J_H \ll U$, J_H is neglected for simplicity in the QMC calculations, and the single-orbital approximation is used to describe the magnetic states of impurities. We calculate magnetic correlations of the impurities using Hirsch-Fye QMC technique with more than 10^6 Monte Carlo sweeps and Matsubara time step $\tau = 0.25$.

III. RESULTS FOR (In, Fe)Sb, (In, Mn)Sb, AND (In, Cr)Sb

The parameters $\epsilon_{\alpha}(\mathbf{k})$ and $V_{\mathbf{i}\xi\mathbf{k}\alpha}$ are obtained by DFT calculations using the WIEN2k package [42]. To reproduce the experimental narrow band gap of 0.17 eV in InSb, we use the modified Becke-Johnson (mBJ) exchange potential [43], which has been implemented in the WIEN2k package. The obtained energy band $\epsilon_{\alpha}(\mathbf{k})$ is shown in Fig. 1, where InSb has space group $F\bar{4}3m$ (No. 216). We obtained a direct gap band $\Delta_g = 0.17$ eV, which is in good agreement with the experimental value [22,26].

A. Results for (In, Fe)Sb

The mixing parameter between ξ orbitals of an Fe impurity and InSb host is defined as $V_{\mathbf{i}\xi\mathbf{k}\alpha} \equiv \langle \phi_{\xi}(\mathbf{i}) | H | \Psi_{\alpha}(\mathbf{k}) \rangle \equiv \frac{1}{\sqrt{N}} e^{i\mathbf{k}\cdot\mathbf{i}} V_{\xi\alpha}(\mathbf{k})$, which can be expressed as

$$V_{\xi\alpha}(\mathbf{k}) = \sum_{\mathbf{o}, \mathbf{n}} e^{i\mathbf{k}\cdot(\mathbf{n}-\mathbf{i})} a_{\mathbf{o}\alpha}(\mathbf{k}) \langle \phi_{\xi}(\mathbf{i}) | H | \phi_{\mathbf{o}}(\mathbf{n}) \rangle, \quad (2)$$

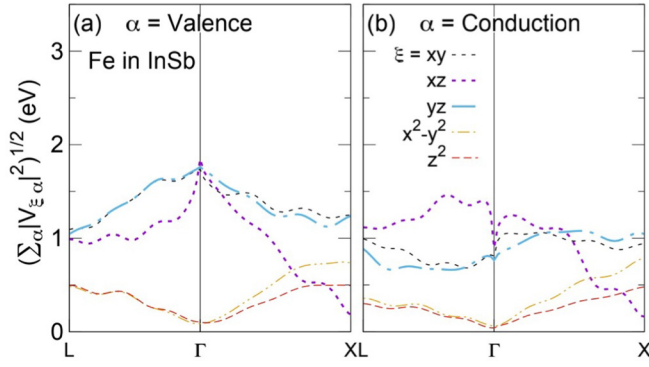


FIG. 2. The mixing function between ξ orbitals of an Fe impurity ($3d$ electrons) and InSb host for (a) valence bands and (b) conduction bands.

where $\phi_\xi(\mathbf{i})$ is the impurity $3d$ state at site \mathbf{i} , and $\Psi_\alpha(\mathbf{k})$ is the host state with wave vector \mathbf{k} and band index α , which is expanded by atomic orbitals $\phi_o(\mathbf{n})$ with orbital index o and site index \mathbf{n} . Here, N is the total number of host lattice sites and $a_{\alpha o}(\mathbf{k})$ is an expansion coefficient. To obtain the mixing integrals of $\langle \phi_\xi(\mathbf{i}) | H | \phi_o(\mathbf{n}) \rangle$, we consider a supercell $\text{In}_{26}\text{FeSb}_{27}$, which is comprised of $3 \times 3 \times 3$ primitive cells, where each primitive cell consists of an InSb, and an In atom is replaced by an Fe atom. The results of the mixing function $V_{\xi\alpha}(\mathbf{k})$ are shown in Fig. 2(a) for valence bands and in Fig. 2(b) for conduction bands. It can be seen that near Γ point the orbitals of d_{xy} , d_{xz} , and d_{yz} contribute more predominantly to the mixing function than the orbitals of $d_{x^2-y^2}$ and d_{z^2} , whereas the contributions of $d_{x^2-y^2}$ and d_{z^2} orbitals to the mixing function increase along Γ to X or L direction.

For $3d$ orbitals of transition metal impurities, the reasonable U is estimated as $U = 4$ eV [17,18,35,36]. The QMC results of the occupation number $\langle n_\xi \rangle$ of a ξ orbital of an Fe impurity in InSb as a function of chemical potential μ at 360 K are shown in Fig. 3. The top of the VB was taken to be zero

and the bottom of the CB to be 0.17 eV. n_ξ is defined as $n_\xi = n_{\xi\uparrow} + n_{\xi\downarrow}$. For Fe $3d$ orbital energy parameter $\varepsilon_d = -2$ eV, a dramatic increase in n_ξ is observed around -0.1 eV for the orbitals $\xi = xy$, xz , and yz , while for $\varepsilon_d = -1$ eV, sharp increases in n_ξ are observed around -0.6 , 0.1 , and 0.2 eV for the orbitals $\xi = z^2$ (or x^2-y^2), yz and xy (or xz), respectively. The sharp increase of n_ξ implies the existence of an impurity bound state (IBS) at this energy ω_{IBS} [35–37,44,45]. Figures 3(b) and 3(d) show the magnetic correlation $\langle M_{1\xi}^z M_{2\xi}^z \rangle$ between ξ orbitals of two Fe impurities with fixed distance R_{12} of the nearest neighbor. The operator $M_{i\xi}^z$ of the ξ orbital at impurity site \mathbf{i} is defined as $M_{i\xi}^z = n_{i\xi\uparrow} - n_{i\xi\downarrow}$. For each ξ orbital, a ferromagnetic (FM) coupling is obtained when the chemical potential μ is close to the IBS position, and the FM correlations become weaker and eventually disappear when μ moves away from the IBS. This role of the IBS in determining the strength of FM correlations between impurities is consistent with the Hartree-Fock and QMC results of various diluted ferromagnetic semiconductors [35–37,44,45].

Recent experiments showed high Curie temperature T_c in n -type semiconductor (In,Fe)Sb [20–22]. In order to reproduce the FM coupling between Fe impurities in semiconductor InSb with n -type carriers, the reasonable $3d$ orbital energy parameter is $\varepsilon_d = -1$ eV, as shown in Fig. 3(d). For n -type carriers, the chemical potential is about $\mu = 0.17$ eV, i.e., near the bottom of the conduction band. The FM coupling between Fe impurities is obtained for $\varepsilon_d = -1$ eV with $\mu = 0.17$ eV as shown in Fig. 3(d), while no stable magnetic coupling between Fe impurities is obtained for $\varepsilon_d = -2$ eV with $\mu = 0.17$ eV as shown in Fig. 3(b). Thus, as a reasonable estimation, we take the parameter $\varepsilon_d = -1$ eV for $3d$ orbitals in our following QMC calculations.

Figures 4(a) and 4(b) show the distance R_{12} dependent magnetic correlation $\langle M_{1\xi}^z M_{2\xi}^z \rangle$ between ξ orbitals of two Fe impurities for the p -type case with $\mu = 0$ eV and for the n -type case with $\mu = 0.2$ eV, respectively. Long-range FM coupling up to approximately 8 \AA ($1.4a_0$) is obtained for the

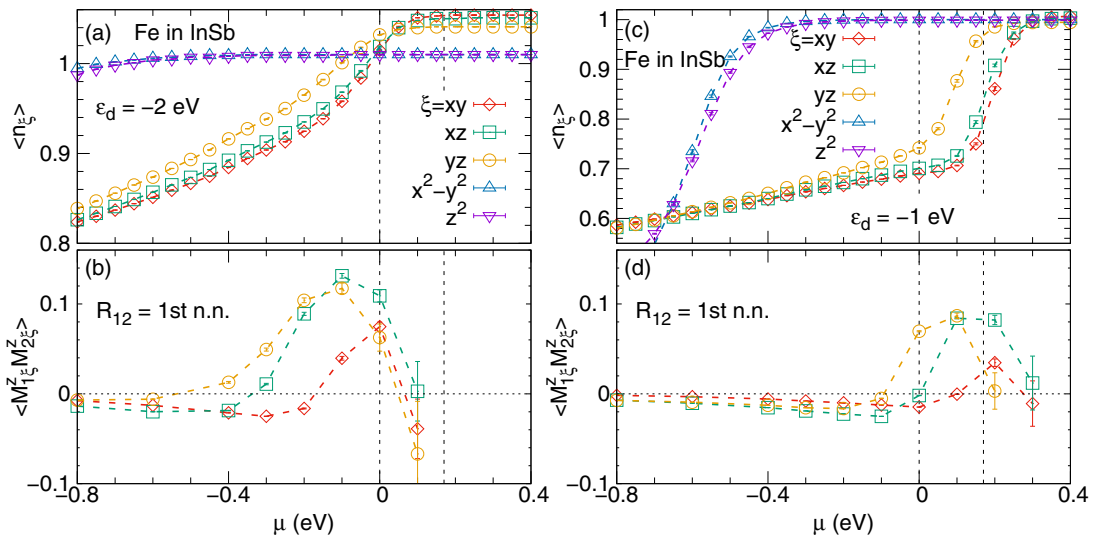


FIG. 3. For Fe-doped InSb, chemical potential μ dependent (a) occupation number $\langle n_\xi \rangle$ of ξ orbital of an Fe impurity, and (b) magnetic correlation $\langle M_{1\xi}^z M_{2\xi}^z \rangle$ between the ξ orbitals of two Fe impurities with fixed distance R_{12} of the first-nearest neighbor at temperature of 360 K with $\varepsilon_d = -2$ eV. (c) and (d) are the same physical quantities as (a) and (b) with $\varepsilon_d = -1$ eV.

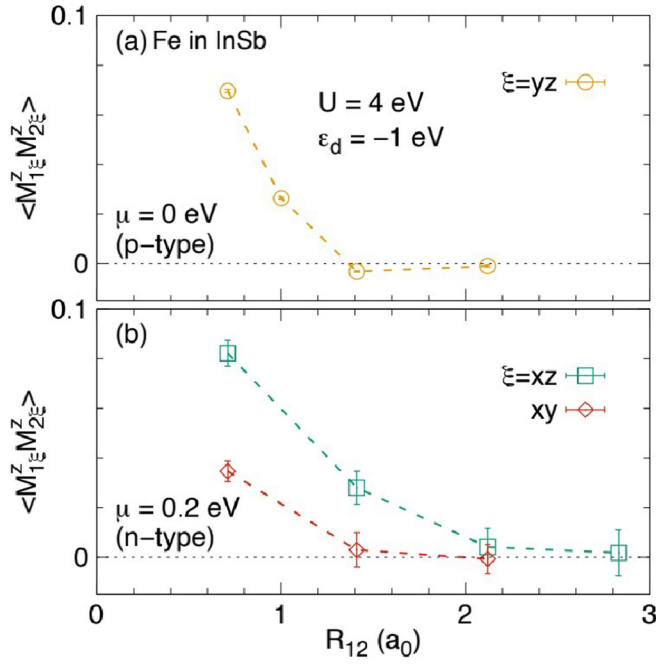


FIG. 4. For Fe-doped InSb, the distance R_{12} dependent magnetic correlation $\langle M_{1\xi}^z M_{2\xi}^z \rangle$ between the ξ orbitals of two Fe impurities for (a) p -type case with chemical potential $\mu = 0$ eV and (b) n -type case with $\mu = 0.2$ eV, where temperature is 360 K.

orbitals $\xi = yz$ for the p -type case with $\mu = 0$ eV. Long-range FM coupling up to approximately 13 \AA ($2a_0$) is obtained for the orbitals $\xi = xz$ as shown in Fig. 4(b) as well. A comparison of Figs. 4(a) and 4(b) shows that the magnitude of FM coupling ($\langle M_{1\xi}^z M_{2\xi}^z \rangle$) in the n -type case is slightly larger than that in the p -type case, which is consistent with the high T_c observed in the n -type semiconductor (In,Fe)Sb in experiments [20–22]. In addition, our calculation in Fig. 4(a) predicts that it is possible to obtain high T_c in semiconductor (In,Fe)Sb with p -type carriers.

B. Results for (In, Mn)Sb

We made similar calculations for Mn-doped InSb. The mixing function between the $3d$ orbitals of Mn impurity and valence and conduction bands of host semiconductor InSb is shown in Fig. 5. It is noted that the mixing parameters are similar to those of Fe-doped InSb as shown in Fig. 2. Figure 6(a) shows the occupation number $\langle n_\xi \rangle$ of ξ orbital of Mn impurity in InSb versus chemical potential μ at temperature 360 K. Sharp increases in n_ξ , which imply the position of IBS ω_{IBS} , were observed around -0.5 eV for $x^2 - y^2$ and z^2 orbitals, and around 0 eV for xy , xz , and yz orbitals, respectively. Figure 6(b) shows the magnetic correlation $\langle M_{1\xi}^z M_{2\xi}^z \rangle$ between ξ orbitals of two Mn impurities as a function of μ , with fixed distance R_{12} as the nearest neighbor. The role of the IBS in determining the strength of FM correlations between impurities is the same as that discussed for Fe-doped InSb in Fig. 3. Figure 7 shows the distance R_{12} dependent magnetic correlation ($\langle M_{1\xi}^z M_{2\xi}^z \rangle$) between ξ orbitals of two Mn impurities for p - and n -type cases. For p -type carriers with $\mu = 0$ eV, the same value used for p -type (In,Fe)Sb, a long-range FM

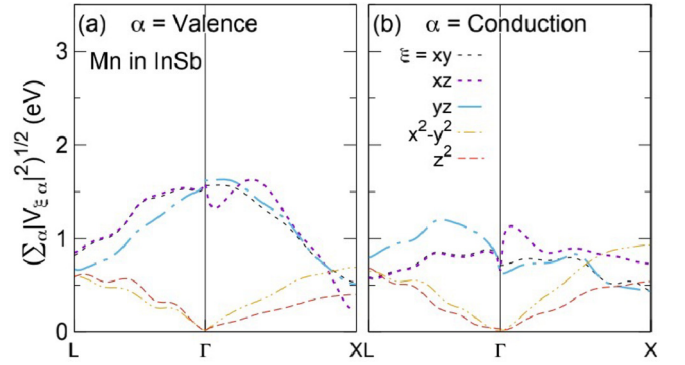


FIG. 5. The mixing function between ξ orbitals of a Mn impurity and InSb host for (a) valence bands and (b) conduction bands.

coupling up to approximately 10 \AA was obtained for $\xi = yz$ orbital, which is longer than 8 \AA obtained for Fe-doped InSb with p -type carriers, while a relatively short-range FM coupling was obtained for the $\xi = xy$ and xz orbitals for p -type case. However, for n -type carriers with $\mu = 0.15$ eV, a weak FM coupling was obtained, as shown in Fig. 7(b). Comparing with Fig. 4 and Fig. 7, we find that the FM couplings in (In, Fe)Sb and (In, Mn)Sb are similar. In experiments, high T_c was obtained in n -type (In,Fe)Sb [20–22], but low T_c was obtained in (In,Mn)Sb [26]. In Sec. VI, we will discuss our understandings in a general picture. In addition, our results predict that a weak FM can exist in semiconductor (In,Mn)Sb with n -type carriers.

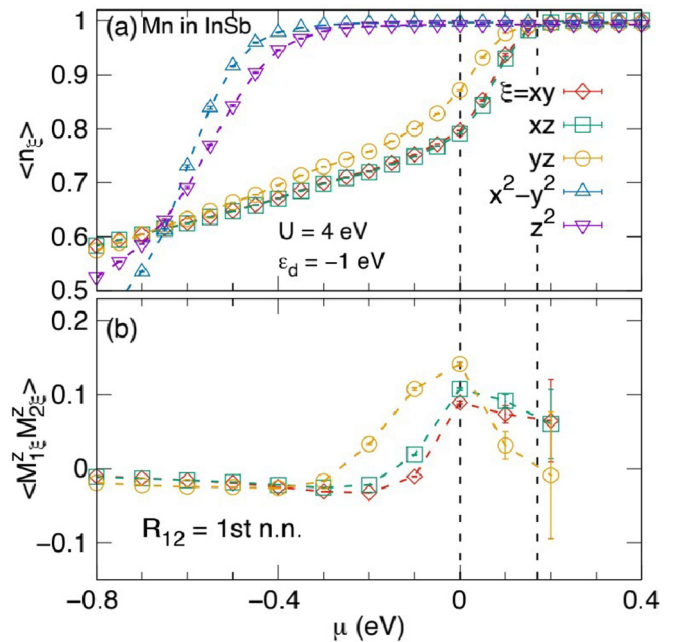


FIG. 6. For Mn-doped InSb, chemical potential μ dependent (a) occupation number $\langle n_\xi \rangle$ of ξ orbital of a Mn impurity, and (b) magnetic correlation $\langle M_{1\xi}^z M_{2\xi}^z \rangle$ between the ξ orbitals of two Mn impurities with fixed distance R_{12} of the first-nearest neighbor at temperature 360 K with $\varepsilon_d = -1$ eV.

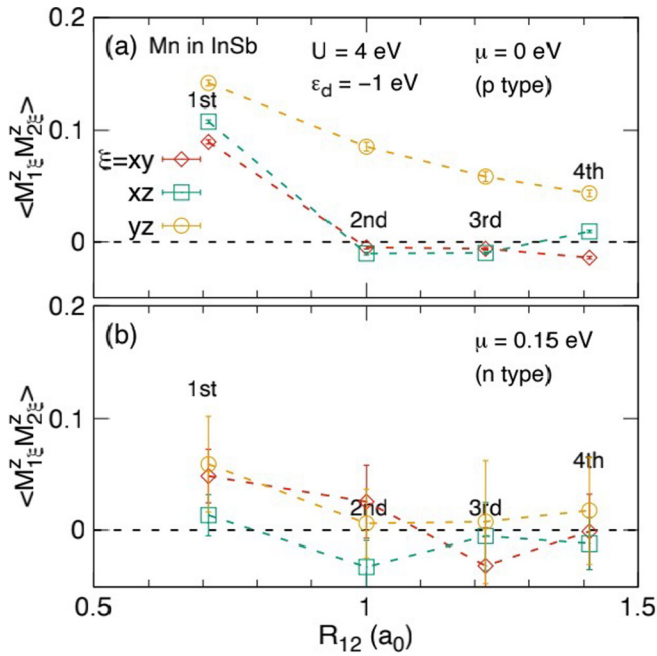


FIG. 7. For Mn-doped InSb, the distance R_{12} dependent magnetic correlation $\langle M_{1\xi}^z M_{2\xi}^z \rangle$ between the ξ orbitals of two Mn impurities for (a) p -type case with chemical potential $\mu = 0$ eV and (b) n -type case with $\mu = 0.15$ eV, where temperature is 360 K.

C. Result for (In, Cr)Sb

We made similar calculations for Cr-doped InSb that have not yet been attempted in experiments. The mixing function between the $3d$ orbitals of Cr impurity and valence and conduction bands of InSb is shown in Fig. 8. Comparing with Figs. 2, 5, and 8, it is clear that the mixing parameters are very similar for Fe, Mn, and Cr-doped InSb. The chemical potential μ dependent occupation number $\langle n_\xi \rangle$ of ξ of a Cr impurity and the magnetic correlation $\langle M_{1\xi}^z M_{2\xi}^z \rangle$ between ξ orbitals of two Cr impurities of the nearest neighbors are shown in Fig. 9. Comparing with Figs. 3(c) and 3(d), 6, and 9, the similar behaviors of IBS and magnetic correlation are obtained for Fe, Mn, and Cr-doped InSb. The distance R_{12} dependent magnetic correlation $\langle M_{1\xi}^z M_{2\xi}^z \rangle$ between ξ orbitals of two Cr impurities with p - and n -type cases is shown in Fig. 10. Comparing

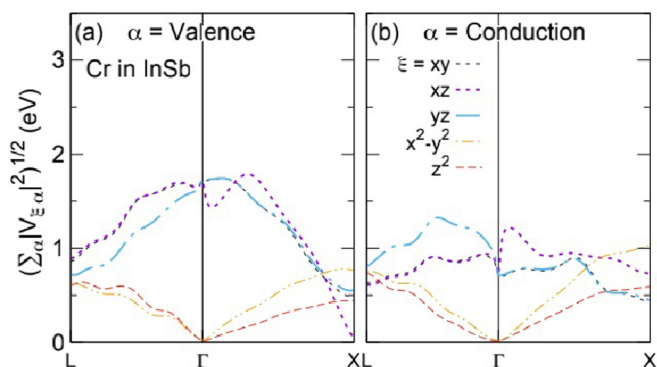


FIG. 8. The mixing function between ξ orbitals of a Cr impurity and InSb host for (a) valence bands and (b) conduction bands.

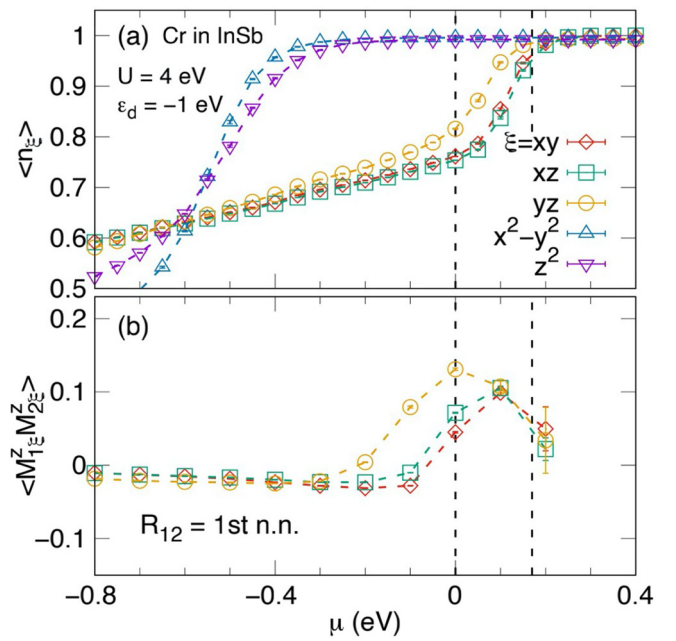


FIG. 9. For Cr-doped InSb, chemical potential μ dependent (a) occupation number $\langle n_\xi \rangle$ of ξ orbital of a Cr impurity, and (b) magnetic correlation $\langle M_{1\xi}^z M_{2\xi}^z \rangle$ between ξ orbitals of two Cr impurities with fixed distance R_{12} of the first-nearest neighbor at temperature 360 K with $\varepsilon_d = -1$ eV.

with Figs. 4, 7, and 10, the similar magnetic correlations are obtained for Fe, Mn, and Cr-doped InSb. Thus, our calculations predict the p - and n -type ferromagnetic semiconductors Cr-doped InSb that possibly have high T_c .

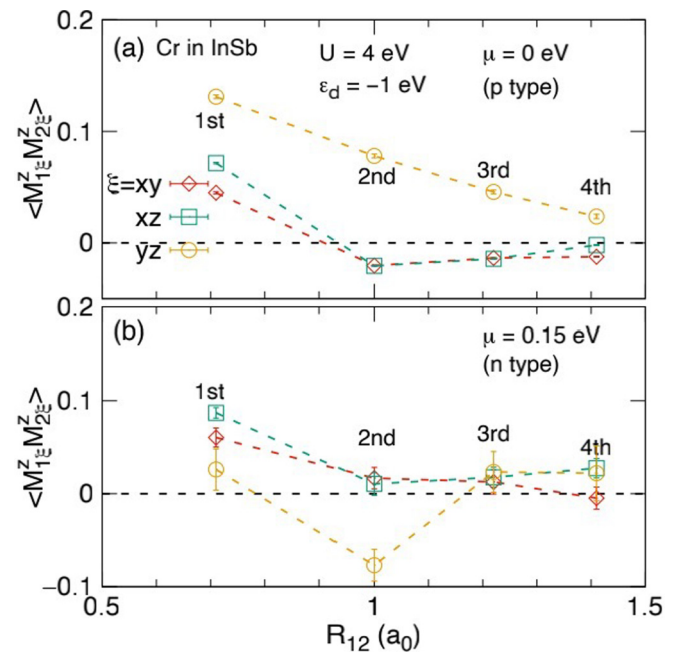


FIG. 10. For Cr-doped InSb, the distance R_{12} dependent magnetic correlation $\langle M_{1\xi}^z M_{2\xi}^z \rangle$ between ξ orbitals of two Cr impurities for (a) p -type case with chemical potential $\mu = 0$ eV and (b) n -type case with $\mu = 0.15$ eV, where temperature is 360 K.

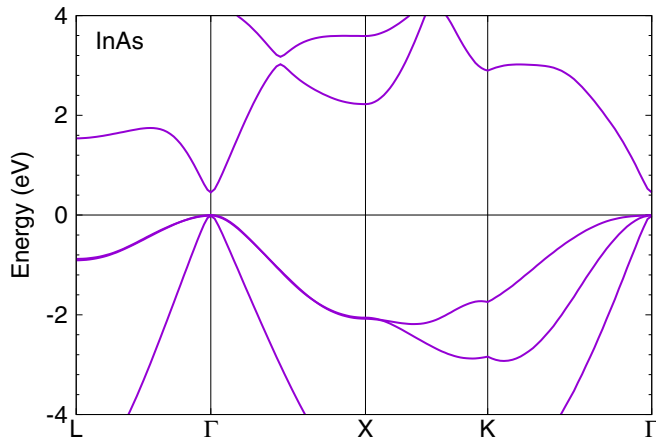


FIG. 11. Energy bands ϵ_α of host InAs, which has the same space group as InSb. A direct band gap of 0.42 eV was obtained by DFT calculations, which agrees well with the experimental value.

IV. RESULTS FOR Fe, Mn, AND Cr-DOPED InAs

InAs has the same space group of $F\bar{4}3m$ (No. 216) as InSb but has a smaller lattice constant of 6.05 Å. By DFT method with the mBJ exchange potential, we calculate the band structure of InAs as shown in Fig. 11. The obtained band gap of 0.42 eV is in a good agreement with the experimental value [27,29].

A. Results for (In, Fe)As

For Fe-doped InAs, chemical potential μ dependent occupation number $\langle n_\xi \rangle$ of ξ orbitals of an Fe impurity and magnetic correlation $\langle M_{1\xi}^z M_{2\xi}^z \rangle$ between ξ orbitals of two Fe impurities of the first-nearest neighbor is shown in Fig. 12. It is shown that the IBS appears at about 0.1 eV for orbitals xy , xz , and yz . The FM correlations between orbitals xy , xz , and yz were obtained when chemical potential μ is close to the position of IBS. The distance R_{12} dependent magnetic correlation $\langle M_{1\xi}^z M_{2\xi}^z \rangle$ between ξ orbitals of two Fe impurities for the p -type case with chemical potential $\mu = 0.1$ eV is shown in Fig. 13. The long range FM coupling between yz orbitals of Fe impurities is obtained. Comparing with Figs. 4 and 13, it is shown that the FM couplings in (In, Fe)Sb and (In, Fe)As are similar. In experiments, high T_c was obtained in n -type (In,Fe)Sb [20–22], but low T_c was obtained in p -type (In,Fe)As [27,28]. In Sec. VI, we give a general picture for this observation.

B. Results for (In, Mn)As

For Mn-doped InAs, chemical potential μ dependent occupation number $\langle n_\xi \rangle$ of ξ orbitals of a Mn impurity and magnetic correlation $\langle M_{1\xi}^z M_{2\xi}^z \rangle$ between ξ orbitals of two Mn impurities of the first-nearest neighbor is shown in Fig. 14. It can be observed that the IBS appears at about 0.1 ~ 0.2 eV for orbitals xy , xz , and yz . The FM correlations between orbitals xy , xz , and yz were obtained when chemical potential μ is close to the position of IBS. The distance R_{12} dependent magnetic correlation $\langle M_{1\xi}^z M_{2\xi}^z \rangle$ between ξ orbitals of two Mn impurities for the p -type case with chemical potential

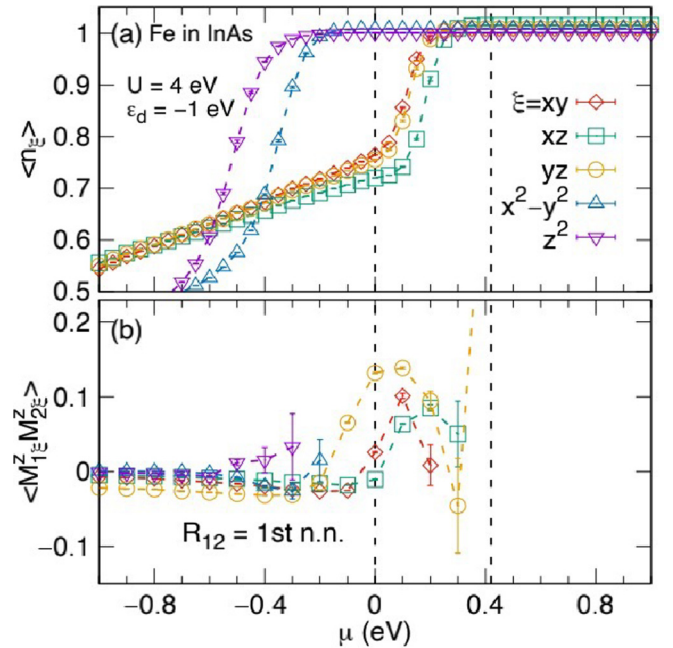


FIG. 12. For Fe-doped InAs, chemical potential μ dependent (a) occupation number $\langle n_\xi \rangle$ of ξ orbital of an Fe impurity, and (b) magnetic correlation $\langle M_{1\xi}^z M_{2\xi}^z \rangle$ between ξ orbitals of two Fe impurities with fixed distance R_{12} of the first-nearest neighbor at temperature of 360 K with $\epsilon_d = -1$ eV.

$\mu = 0.1$ eV is shown in Fig. 15. The long range FM coupling between yz orbitals of Mn impurities is obtained. Comparing with Figs. 13 and 15, we uncover that the FM couplings in (In,Fe)As and (In,Mn)As are similar. In experiments, low and similar T_c were obtained in n -type (In,Fe)As [27,28] and p -type (In,Mn)As [29]. The detail discussions will be presented in Sec. VI.

C. Results for (In, Cr)As

For Cr-doped InAs, the chemical potential μ dependent occupation number $\langle n_\xi \rangle$ of a Cr impurity and the magnetic correlation $\langle M_{1\xi}^z M_{2\xi}^z \rangle$ between ξ orbitals of two Cr impurities of the first nearest neighbor are shown in Fig. 16.

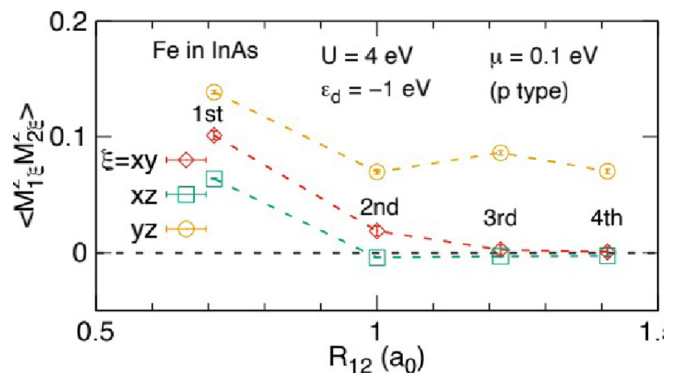


FIG. 13. For Fe-doped InAs, the distance R_{12} dependent magnetic correlation $\langle M_{1\xi}^z M_{2\xi}^z \rangle$ between ξ orbitals of two Fe impurities for the p -type case with chemical potential $\mu = 0.1$ eV, where temperature is 360 K.

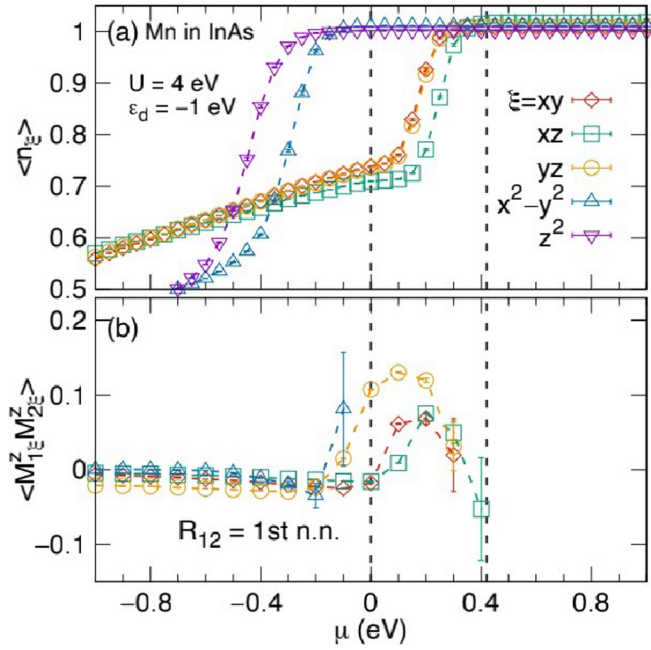


FIG. 14. For Mn-doped InAs, chemical potential μ dependent (a) occupation number $\langle n_{\xi} \rangle$ of ξ orbital of a Mn impurity, and (b) magnetic correlation $\langle M_{1\xi}^z M_{2\xi}^z \rangle$ between ξ orbitals of two Mn impurities with fixed distance R_{12} of the first-nearest neighbor at temperature of 360 K with $\varepsilon_d = -1$ eV.

Comparing with Figs. 12, 14, and 16, similar behaviors of IBS and magnetic correlation are obtained for Fe, Mn, Cr-doped InAs. The distance R_{12} dependent magnetic correlation $\langle M_{1\xi}^z M_{2\xi}^z \rangle$ between ξ orbitals of two Cr impurities with p -type carriers is shown in Fig. 17. Comparing with Figs. 13, 15, and 17, similar magnetic correlations are also obtained for Fe, Mn, Cr-doped InAs. Thus, our calculations predict a ferromagnetic semiconductor Cr-doped InAs with p -type carriers.

V. RESULTS FOR Fe, Mn, AND Cr DOPED GaSb

GaSb has the same space group of $F\bar{4}3m$ (No. 216) as InSb but has a smaller lattice constant of 6.09 Å. By DFT method with the mBJ exchange potential, we calculate the

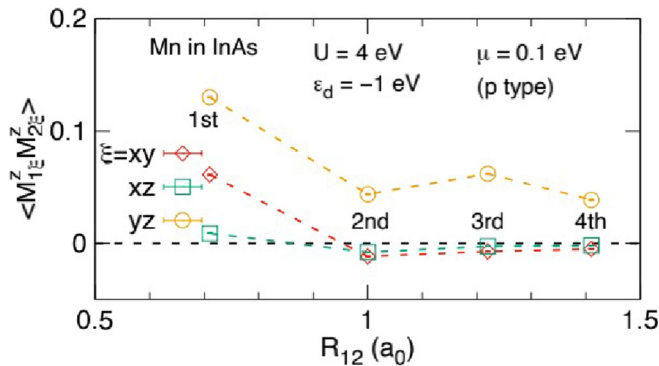


FIG. 15. For Mn-doped InAs, the distance R_{12} dependent magnetic correlation $\langle M_{1\xi}^z M_{2\xi}^z \rangle$ between ξ orbitals of two Mn impurities for the p -type case with chemical potential $\mu = 0$ eV, where temperature is 360 K.

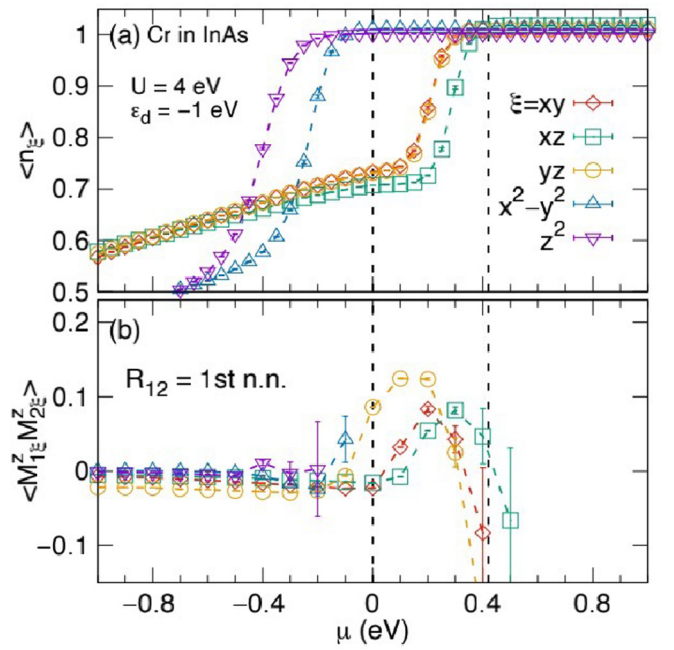


FIG. 16. For Cr-doped InAs, chemical potential μ dependent (a) occupation number $\langle n_{\xi} \rangle$ of ξ orbital of a Cr impurity, and (b) magnetic correlation $\langle M_{1\xi}^z M_{2\xi}^z \rangle$ between ξ orbitals of two Cr impurities with fixed distance R_{12} of the first-nearest neighbor at temperature 360 K with $\varepsilon_d = -1$ eV.

band structure of GaSb as shown in Fig. 18. The obtained band gap of 0.75 eV is in a good agreement with the experimental value [13,25].

A. Results for (Ga, Fe)Sb

For Fe-doped GaSb, chemical potential μ dependent occupation number $\langle n_{\xi} \rangle$ of ξ orbitals of an Fe impurity and magnetic correlation $\langle M_{1\xi}^z M_{2\xi}^z \rangle$ between ξ orbitals of two Fe impurities of the first-nearest neighbor is shown in Fig. 19. It is shown that the IBS appears at about 0.1 eV for orbital yz and about 0.25 eV for xz and xy orbitals. The FM correlations between orbitals xy , xz , and yz were obtained when chemical

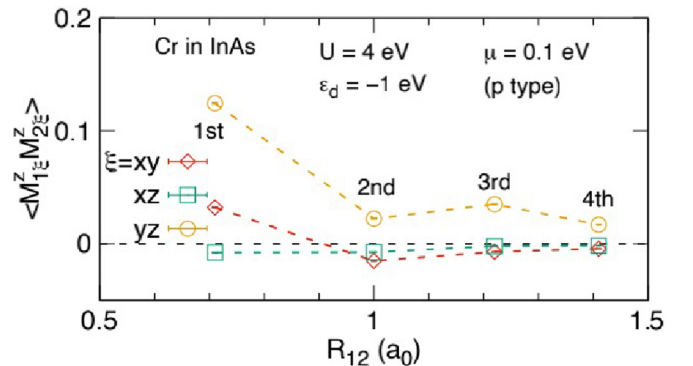


FIG. 17. For Cr-doped InAs, the distance R_{12} dependent magnetic correlation $\langle M_{1\xi}^z M_{2\xi}^z \rangle$ between ξ orbitals of two Cr impurities for the p -type case with chemical potential $\mu = 0.1$ eV, where temperature is 360 K.

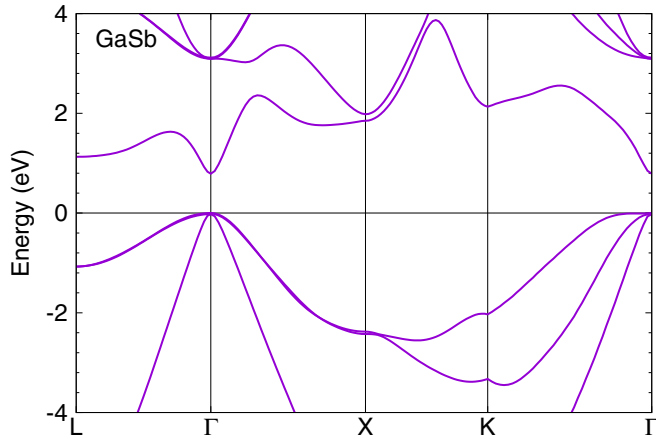


FIG. 18. Energy bands ϵ_α of host GaSb, which has the same space group as InSb. A direct band gap of 0.75 eV was obtained by DFT calculations, which agrees well with the experimental value.

potential μ is close to the position of IBS. The distance R_{12} dependent magnetic correlation $\langle M_{1\xi}^z M_{2\xi}^z \rangle$ between ξ orbitals of two Fe impurities for the p -type case with chemical potential $\mu = 0$ eV is shown in Fig. 20. The long range FM coupling between yz orbitals of Fe impurities is obtained, which is consistent with the high T_c observed in the p -type semiconductor (Ga,Fe)Sb in experiments [13–16].

B. Results for (Ga, Mn)Sb

For Mn-doped GaSb, chemical potential μ dependent occupation number $\langle n_\xi \rangle$ of ξ orbitals of a Mn impurity and

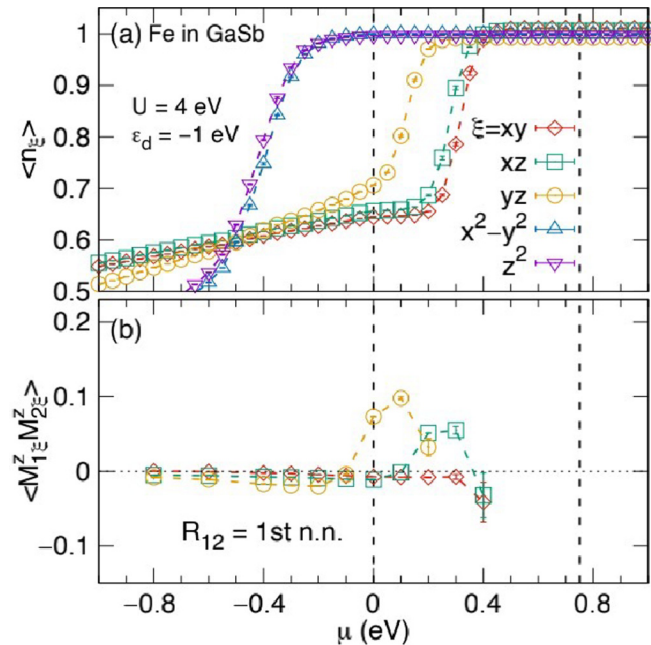


FIG. 19. For Fe-doped GaSb, chemical potential μ dependent (a) occupation number $\langle n_\xi \rangle$ of ξ orbital of an Fe impurity, and (b) magnetic correlation $\langle M_{1\xi}^z M_{2\xi}^z \rangle$ between ξ orbitals of two Fe impurities with fixed distance R_{12} of the first-nearest neighbor at temperature of 360 K with $\epsilon_d = -1$ eV.

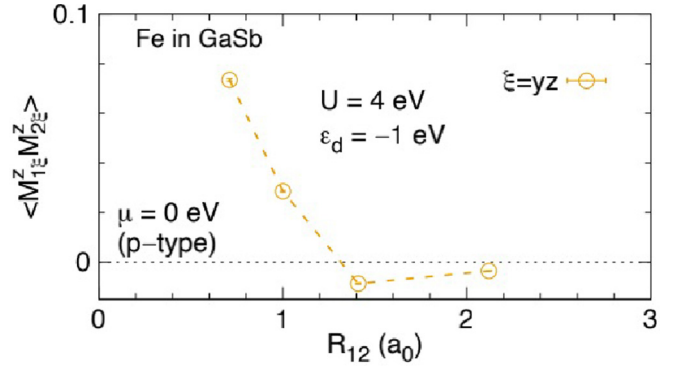


FIG. 20. For Fe-doped GaSb, the distance R_{12} dependent magnetic correlation $\langle M_{1\xi}^z M_{2\xi}^z \rangle$ between ξ orbitals of two Fe impurities for the p -type case with chemical potential $\mu = 0.1$ eV, where temperature is 360 K.

magnetic correlation $\langle M_{1\xi}^z M_{2\xi}^z \rangle$ between ξ orbitals of two Mn impurities of the first-nearest neighbor is shown in Fig. 21. It is shown that the IBS appears at about 0.1 eV for orbitals xy , xz , and yz . The FM correlations between orbitals xy , xz , and yz were obtained when chemical potential μ is close to the position of IBS. The distance R_{12} dependent magnetic correlation $\langle M_{1\xi}^z M_{2\xi}^z \rangle$ between ξ orbitals of two Mn impurities for the p -type case with chemical potential $\mu = 0.1$ eV is shown in Fig. 22. The long range FM coupling between yz orbitals of Mn impurities is obtained. Comparing with Figs. 19 and 21, one may find that the FM couplings in (Ga, Fe)Sb and (Ga,Mn)Sb are similar. In experiments, high T_c was obtained in p -type (Ga,Fe)Sb [13–16], but low T_c was obtained in

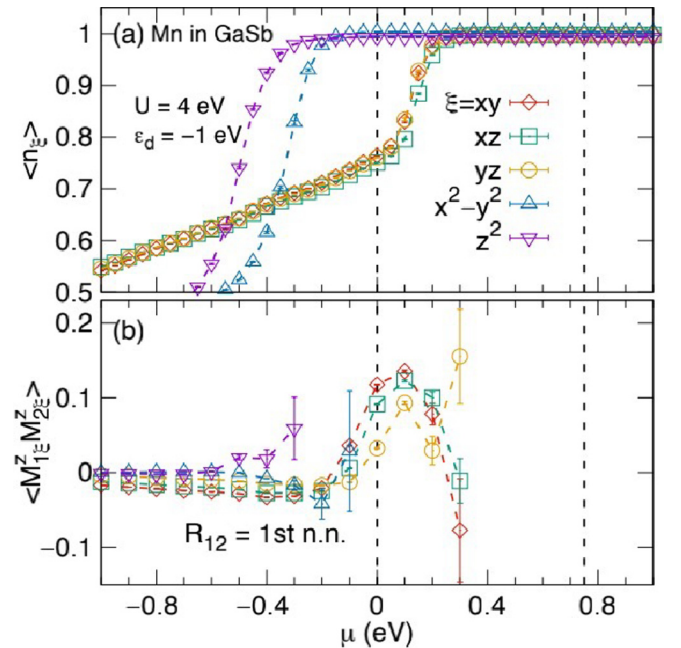


FIG. 21. For Mn-doped GaSb, chemical potential μ dependent (a) occupation number $\langle n_\xi \rangle$ of ξ orbital of an Mn impurity, and (b) magnetic correlation $\langle M_{1\xi}^z M_{2\xi}^z \rangle$ between ξ orbitals of two Mn impurities with fixed distance R_{12} of the first-nearest neighbor at temperature of 360 K with $\epsilon_d = -1$ eV.

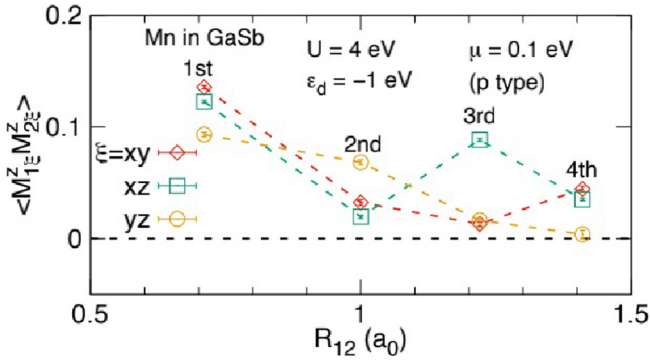


FIG. 22. For Mn-doped GaSb, the distance R_{12} dependent magnetic correlation $\langle M_{1\xi}^z M_{2\xi}^z \rangle$ between ξ orbitals of two Mn impurities for the p -type case with chemical potential $\mu = 0.1$ eV, where temperature is 360 K.

p -type (Ga,Mn)Sb [25]. To resolve this puzzling situation, in Sec. VI we will discuss this issue in a general picture.

C. Results for (Ga, Cr)Sb

For Cr-doped GaSb, the chemical potential μ dependent occupation number $\langle n_\xi \rangle$ of a Cr impurity and the magnetic correlation $\langle M_{1\xi}^z M_{2\xi}^z \rangle$ between ξ orbitals of two Cr impurities of the first nearest neighbor are shown in Fig. 23. Comparing with Figs. 19, 21, and 23, similar behaviors of IBS and magnetic correlation are obtained for Fe, Mn, and Cr-doped GaSb. The distance R_{12} dependent magnetic correlation $\langle M_{1\xi}^z M_{2\xi}^z \rangle$ between ξ orbitals of two Cr impurities with p -type carriers is

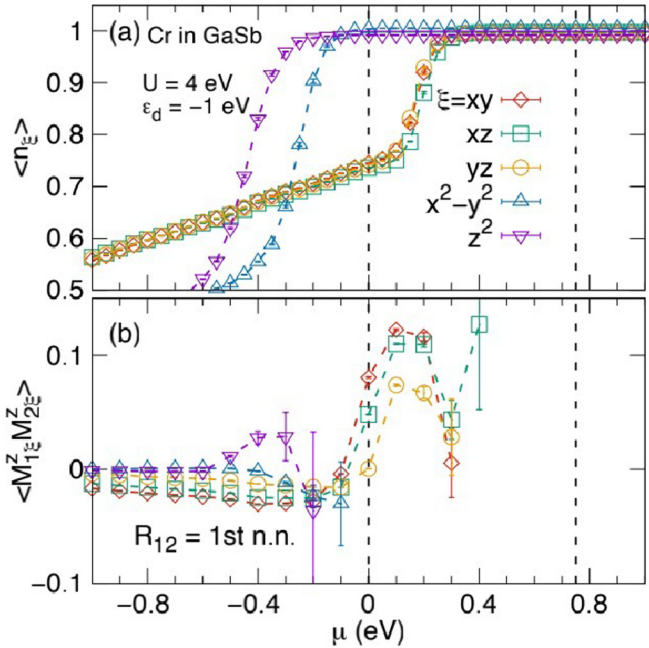


FIG. 23. For Cr-doped GaSb, chemical potential μ dependent (a) occupation number $\langle n_\xi \rangle$ of ξ orbital of a Cr impurity, and (b) magnetic correlation $\langle M_{1\xi}^z M_{2\xi}^z \rangle$ between ξ orbitals of two Cr impurities with fixed distance R_{12} of the first-nearest neighbor at temperature of 360 K with $\varepsilon_d = -1$ eV.

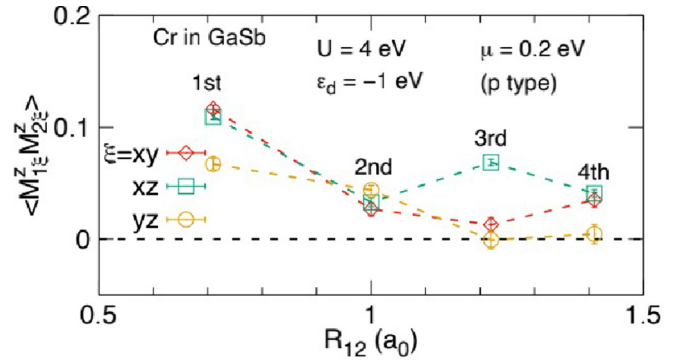


FIG. 24. For Cr-doped GaSb, the distance R_{12} dependent magnetic correlation $\langle M_{1\xi}^z M_{2\xi}^z \rangle$ between ξ orbitals of two Cr impurities for the p -type case with chemical potential $\mu = 0.2$ eV, where temperature is 360 K.

shown in Fig. 24. Comparing with Figs. 20, 22, and 24, similar magnetic correlations are obtained for Fe, Mn, Cr-doped GaSb. Thus, our calculations predict the p -type ferromagnetic semiconductor Cr-doped GaSb could have high T_c .

VI. DISCUSSION

To understand the mechanism of ferromagnetism in these ferromagnetic semiconductors, we list the results of the maximum $\langle M_{1\xi}^z M_{2\xi}^z \rangle$ between two impurities with the first nearest neighbor (n.n.) in Table I. The value of the maximum $\langle M_{1\xi}^z M_{2\xi}^z \rangle$ for impurities Fe, Mn, and Cr is, respectively, about 0.1, 0.13, and 0.12 for p -type semiconductor GaSb, about 0.14, 0.13, and 0.12 for p -type semiconductor InAs and about 0.09, 0.07, and 0.08 for n -type semiconductor InSb. It is noted that different values of the maximum $\langle M_{1\xi}^z M_{2\xi}^z \rangle$ are obtained for different impurities in p -type InSb. The maximum $\langle M_{1\xi}^z M_{2\xi}^z \rangle$ for impurities Fe, Mn, and Cr is, respectively, about 0.07, 0.14, and 0.13 for p -type semiconductor InSb. In general, the results suggest that for the same host semiconductors, impurities Fe, Mn, and Cr have quite similar magnetic correlation $\langle M_{1\xi}^z M_{2\xi}^z \rangle$. The results in Table I are calculated based on the Anderson impurity model in the diluted impurity limit. Based on these results, we argue that high (low) T_c in these ferromagnetic semiconductors in experiments may come from high (low) impurity concentrations,

TABLE I. The DFT+QMC calculation results of the maximum value of $\langle M_1 M_2 \rangle$ between two impurities with the first nearest neighbor (n.n.) for Fe, Mn, and Cr-doped InSb, InAs, and GaSb.

The maximum $\langle M_1 M_2 \rangle$ at the first n.n.	Host semiconductors		
	InSb (gap=0.17eV)	InAs (gap=0.42eV)	GaSb (gap=0.75eV)
Fe	0.07 (p -type) 0.09 (n -type)	0.14 (p -type)	0.1 (p -type)
Mn	0.14 (p -type) 0.07 (n -type)	0.13 (p -type)	0.13 (p -type)
Cr	0.13 (p -type) 0.08 (n -type)	0.12 (p -type)	0.12 (p -type)

TABLE II. The experimental results of Curie temperature, impurity concentration, carrier type, and band gap for some ferromagnetic semiconductors.

Ferromagnetic semiconductors	Curie temperature, T_c (K)	Impurity concentration, N_m	Carrier types	Band gap (eV)	Reference of experiments (years)
(Ga,Fe)Sb	340	25%	<i>p</i> -type	0.75	Ref. [13] (2016)
(Ga,Mn)Sb	25	2.3%	<i>p</i> -type	0.75	Ref. [25] (2000)
(In,Fe)Sb	385	35%	<i>n</i> -type	0.17	Ref. [22] (2019)
(In,Mn)Sb	10	4%	<i>p</i> -type	0.17	Ref. [26] (2008)
(In,Fe)As	70	8%	<i>n</i> -type	0.42	Ref. [27] (2012)
(In,Mn)As	90	10%	<i>p</i> -type	0.42	Ref. [29] (2006)
(Ba, K)(Zn, Mn) ₂ As ₂	230	15%	<i>p</i> -type	0.2	Ref. [9] (2014)
Ba(Zn, Co) ₂ As ₂	45	4%	<i>n</i> -type	0.2	Ref. [24] (2019)
Li(Zn,Mn)As	50	10%	<i>p</i> -type	1.6	Ref. [6] (2011)
Li(Zn,Mn)P	34	10%	<i>p</i> -type	2.0	Ref. [7] (2013)
Li(Cd,Mn)P	45	10%	<i>p</i> -type	1.3	Ref. [46] (2019)
(Ga,Mn)As	200	16%	<i>p</i> -type	1.4	Ref. [3] (2011)

rather than from the impurity-impurity magnetic correlations themselves.

To further check our argument, in Table II we list the experimental results of Curie temperature T_c and the impurity concentrations N_m in some ferromagnetic semiconductors. From Table II, it is observed that for the same host semiconductors with different impurities, T_c is naively proportional to the impurity concentration N_m . For example, $T_c = 340$ K, $N_m = 25\%$ for Fe-doped GaSb, and $T_c = 25$ K, $N_m = 2.3\%$ for Mn-doped GaSb. More examples are available in Table II, such as $T_c = 70$ K, $N_m = 8\%$ for Fe-doped InAs, and $T_c = 90$ K, $N_m = 10\%$ for Mn-doped InAs; $T_c = 230$ K, $N_m = 15\%$ for Mn-doped BaZn₂As₂, and $T_c = 45$ K, $N_m = 4\%$ for Co-doped BaZn₂As₂. Certainly, this relation is not numerically exact, and the deviation from this relation exists. For example, $T_c = 385$ K, $N_m = 35\%$ for Fe-doped InSb, and $T_c = 10$ K, $N_m = 4\%$ for Mn-doped InSb. In order to increase T_c in diluted ferromagnetic semiconductors, our results suggest that a primary strategy is to increase the impurity concentrations. For this purpose, it is crucial to choose proper impurities and semiconductor hosts to avoid valence state mismatch during the magnetic doping.

Our numerical results show that the reason that (Ga,Fe)Sb and (In,Fe)Sb have high T_c in the experiments [13,22] is from high impurity concentrations of Fe impurities. The Fe impurities in GaSb and InSb do not introduce additional carriers [13,22], which means that there is no valence mismatch between Fe³⁺ and Ga³⁺ and In³⁺, and Fe impurities can

be doped to vary high concentrations (25% to 35% in Table II). In contrast, Mn impurities in GaSb and InSb is Mn²⁺ and cannot be doped in a high concentration due to valence mismatch.

Therefore, the origin of high T_c in (Ga,Fe)Sb and (In,Fe)Sb is not due to the carrier induced mechanism because Fe³⁺ does not introduce carriers. The calculations show that ferromagnetism appears in both *p*- and *n*-type semiconductors with narrow band gaps and in only *p*-type semiconductors with wide band gaps, which is consistent with our previous theory [17–19] and experimental observations in most of ferromagnetic semiconductors.

VII. CURIE TEMPERATURE BY MEAN FIELD THEORY

We estimate the Curie temperature T_c from a simple Weiss mean-field formula:

$$T_c = \frac{2}{3k_B} S(S+1) \sum_i z_i J_i, \quad (3)$$

where z_i is the coordination number and J_i are the exchange couplings of the i th nearest neighbors. To obtain the exchange couplings, as an approximation, we map the ferromagnetic correlation between impurities onto the isotropic Heisenberg model for two particles with five d orbitals

$$H = -J \sum_{\zeta, \eta=d} \mathbf{S}_{1\zeta} \cdot \mathbf{S}_{2\eta}, \quad (4)$$

where $\mathbf{S}_{1\zeta}$ represents the spin-1/2 operator of ζ ($= d_{xy}, d_{xz}, d_{yz}, d_{x^2-y^2}$ or d_{z^2}) orbital. At finite temperature, by defining $\beta = 1/k_B T$ with k_B the Boltzmann constant, we write down

TABLE IV. The Curie temperatures corresponding to three different doping concentrations of 12.5%, 25%, and 37.5% for *n*-type Fe-doped InSb.

Doping concentration	12.5%	25%	37.5%
T_c (K)	120	245	379

TABLE III. The $\langle M_1^z M_2^z \rangle$ and the effective exchange J_i extracted from DFT+QMC calculations between two Fe impurities with different nearest neighbor (n.n.) for *n*-type Fe-doped InSb with spin $S = 5/2$. We have only plotted $\langle M_{1\zeta}^z M_{2\eta}^z \rangle$ with $\zeta = \eta = d_{xz}, d_{yz}$ in Fig. 4(b), because the orbital-orbital correlation $\langle M_{1\zeta}^z M_{2\eta}^z \rangle$ for other ζ and η orbitals are calculated to be very small and negligible.

The i th n.n.	First	Second	Third	Fourth
$\langle M_1^z M_2^z \rangle$ ($10^{-2} \mu_B^2$)	0.467	0.231	0.155	0.124
J_i/k_B (K)	6.757	3.334	2.235	1.788

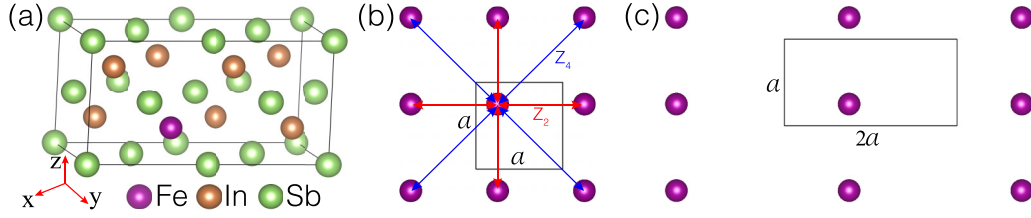


FIG. 25. (a) 12.5% doping concentration for Fe-doped InSb in a supercell of InSb containing eight In atoms and the views from (b) [100] and (c) [001] directions, where we have only plotted the magnetic atoms (Fe atoms) and the supercell is indicated.

the orbital-orbital correlation as

$$\langle S_{1m}^z S_{2n}^z \rangle = \text{Tr}(S_{1m}^z S_{2n}^z e^{-\beta H}) / \text{Tr}(e^{-\beta H}), \quad (5)$$

where S_i^z represents the z component of spin S_i . Considering

$$\begin{aligned} \mathbf{S}_{1\zeta} \cdot \mathbf{S}_{2\eta} &= \frac{1}{2} [(\mathbf{S}_{1\zeta} + \mathbf{S}_{2\eta})^2 - \mathbf{S}_{1\zeta}^2 - \mathbf{S}_{2\eta}^2] \\ &= \frac{1}{2} [S_{\zeta\eta}(S_{\zeta\eta} + 1) - 2s(s + 1)], \end{aligned} \quad (6)$$

where $s = 1/2$, $S_{\zeta\eta} = 0, 1$, and the trace could be taken as summation:

$$\begin{aligned} \text{Tr}(\dots) &= \prod_{\zeta, \eta} \left[\sum_{S_{\zeta\eta}=0}^1 \sum_{S_{\zeta\eta}=-S_{\zeta\eta}}^{S_{\zeta\eta}} \right] (\dots) \\ &= \prod_{\zeta, \eta} \left[\sum_{S_{1\zeta}^z=-1/2}^{1/2} \sum_{S_{2\eta}^z=-1/2}^{1/2} \right] (\dots), \quad (7) \\ \text{Tr}(e^{-\beta H}) &= \left[\sum_{S_{mn}=0}^1 \sum_{S_{mn}^z=-S_{mn}}^{S_{mn}} e^{\beta J S_{1m} S_{2n}} \right] \\ &\quad \times \prod_{\zeta, \eta \neq m, n} \left[\sum_{S_{\zeta\eta}=0}^1 \sum_{S_{\zeta\eta}=-S_{\zeta\eta}}^{S_{\zeta\eta}} e^{\beta J S_{1\zeta} S_{2\eta}} \right], \quad (8) \end{aligned}$$

we have

$$\langle S_{1m}^z S_{2n}^z \rangle = \frac{1}{4} \cdot \frac{1 - e^{-\beta J}}{3 + e^{-\beta J}}. \quad (9)$$

We define the average of impurity-impurity correlation $\langle M_1^z M_2^z \rangle = \sum_{\zeta, \eta=d} \langle M_{1\zeta}^z M_{2\eta}^z \rangle / (2S)^2$, where spin $S = \langle n \rangle / 2 = \sum_{\xi} \langle n_{\xi} \rangle / 2$, and the results of $\langle M_1^z M_2^z \rangle$ extracted from our QMC calculation results are listed in Table III. The unit of $\langle M_1^z M_2^z \rangle$ is $1^2 = (2s)^2 = 4(\mu_B)^2$ and μ_B is Bohr magneton. To be consistent with our QMC calculation results, whose unit of $\langle M_1^z M_2^z \rangle$ is μ_B^2 , the average of impurity-impurity correlation can be obtained as $\langle M_1^z M_2^z \rangle = 4 \langle S_{1m}^z S_{2n}^z \rangle$. Thus, for a given temperature if we have the average of impurity-impurity correlation

TABLE V. The Curie temperatures corresponding to three different doping concentrations of 12.5%, 25%, and 37.5% for p -type Cr-doped InSb, InAs, and GaSb.

Doping concentration		12.5%	25%	37.5%
T_c (K)	(In,Cr)Sb	62	214	406
	(In,Cr)As	17	129	264
	(Ga,Cr)Sb	242	534	851

$\langle M_1^z M_2^z \rangle$, we can deduce an effective exchange J between two impurities.

In the following, we shall take the n -type (In,Fe)Sb as an example to investigate the impurity concentration dependent Curie temperature. The total spin for n -type (In,Fe)Sb is $S = \langle n \rangle / 2 = 5/2$ as shown in Fig. 3(c). The impurity-impurity correlation $\langle M_1^z M_2^z \rangle$ between two Fe impurities as a function of the distance between two Fe impurities and the effective exchange J_i of the i th n.n. are listed in Table III, where we only consider four kinds of n.n. hoppings with the n.n. $R_1 = (0.5, 0, 0.5)a$, the next n.n. $R_2 = (1, 0, 0)a$, the third n.n. $R_3 = (1, 0.5, 0.5)a$, and the fourth n.n. $R_4 = (1, 1, 0)a$.

To simulate different doping concentrations, for simplicity, we consider three different doping concentrations (Nm) of 12.5%, 25%, and 37.5% in a supercell of InSb containing eight In atoms [two unit cells of Fig. 1(a)]. In this case the three different doping concentrations correspond to one, two, and three Fe atom impurities, respectively. If we consider larger supercells, these three concentrations will hold more doping configurations, which are too complicated situations and we shall not study them here. Let us first investigate the 12.5% doping concentration, i.e., one In atom was replaced by a Fe impurity in the InSb supercell as shown in Fig. 25(a). In this case, from Figs. 25(b) and 25(c), one may observe that the Fe impurities form a two-dimensional square lattice with the lattice constant a (R_2), so the coordination numbers $z_i = \{0, 4, 0, 4\}$ with $i = \{1, 2, 3, 4\}$. Thus, combining Eq. (3) and Table III we can estimate the Curie temperature to be 120 K for 12.5% n -type Fe-doped InSb. For 25% doping concentration, i.e., two Fe impurities in the InSb supercell containing eight In atoms, there are 28 doping configurations, among which only three are inequivalent with the probability of 5/7, 1/7, and 1/7, respectively, giving rise to a Curie temperature by Eq. (3) of 250.5, 241.8, and 223.8 K, respectively. Thus, the average Curie temperature can be estimated to be 245 K for 25% n -type Fe-doped InSb. For 37.5% doping

TABLE VI. The $\langle M_1^z M_2^z \rangle$ and the effective exchange J_i extracted from DFT+QMC calculations between two Fe impurities with different nearest neighbor (n.n.) for n -type Fe-doped InSb with spin $S = 5/2$ at temperatures of 240 and 480 K.

The i th n.n.		First	Second	Third	Fourth
240 K	$\langle M_1^z M_2^z \rangle$ ($10^{-2} \mu_B^2$)	0.683	0.394	0.239	0.134
	J_i/k_B (K)	6.602	3.797	2.300	1.288
480 K	$\langle M_1^z M_2^z \rangle$ ($10^{-2} \mu_B^2$)	0.376	0.122	0.136	0.114
	J_i/k_B (K)	7.247	2.345	2.615	2.191

TABLE VII. The Curie temperatures corresponding to three different doping concentrations of 12.5%, 25%, and 37.5% for n -type Fe-doped InSb at temperatures of 240 and 480 K for QMC calculation.

QMC temperature	Doping concentration	12.5%	25%	37.5%
240 K	T_c (K)	119	242	373
480 K		106	246	392

concentration, i.e., three In atoms were replaced by three Fe impurities in the InSb supercell containing eight In atoms. There are 56 doping configurations, among which only four are inequivalent. The probability of the four different doping methods is $2/7$, $2/7$, $1/7$, and $2/7$, respectively. They give rise to a Curie temperature by Eq. (3) of 399.3, 375.7, 375.7, and 363.7 K, respectively. Thus, the average Curie temperature can be estimated to be 379 K for 37.5% n -type Fe-doped InSb. These results are summarized in Table IV. Our estimated Curie temperature of 379 K for 37.5% n -type Fe-doped InSb is comparable with the experimental Curie temperature of 385 K for 35% n -type Fe-doped InSb in Table II.

By using the above method and combining the QMC results in Figs. 10, 17, and 24, we estimate the Curie temperatures corresponding to three different doping concentration of 12.5%, 25%, and 37.5% for p -type Cr-doped InSb, InAs, and GaSb as listed in Table V. From Table V, we find that p -type Cr-doped InSb, InAs, and GaSb ferromagnetic semiconductors may have high T_c with a high doping concentration, especially for p -type Cr-doped GaSb.

To investigate the temperature dependent magnetic correlation, we have also performed the QMC calculation at 240 K and 480 K. The results are summarized in Table VI. One may observe that the magnetic correlation decreases with increasing temperature. With the mean-field theory, we also estimate the Curie temperatures as listed in Table VII at these two QMC simulation temperatures, respectively, which are comparable with the results as listed in Table IV. This shows that our calculations are reasonable and the results are robust.

For the cases with 100% of magnetic impurities, such as FeSb and CrSb, our calculations show that both are ferromagnetic metals. It is noted that the mobility of electrons and holes in InSb is nine and two times higher than that in GaAs, respectively [47,48]. The mobility could be another figure of

merit for InSb and related magnetic semiconductors, which is left for future study.

VIII. SUMMARY

By the combined method of density functional theory and quantum Monte Carlo, we have systematically studied the ferromagnetism of Fe, Mn, Cr-doped GaSb, InSb, and InAs magnetic semiconductors. In the diluted impurity limit, our calculations show that the impurities Fe, Mn, and Cr have similar magnetic correlations in the same host semiconductors. We predict that ferromagnetic semiconductors of Cr-doped InSb, InAs, and GaSb may have possibly high T_c . More importantly, our results imply that high (low) T_c obtained in these experiments mainly come from high (low) impurity concentrations rather than the magnetic correlations between impurities. In addition, our results show that the origin of high T_c in (Ga,Fe)Sb and (In,Fe)Sb is not due to the carrier induced mechanism because Fe^{3+} does not introduce carriers. In order to increase the Curie temperature in diluted ferromagnetic semiconductors, our results suggest that an alternative tactics is to increase the impurity concentrations, such as by choosing proper impurities and host semiconductors to avoid valence state mismatch during the magnetic doping.

ACKNOWLEDGMENTS

The authors thank valuable discussions with Prof. M. Tanaka on related experiments. This work is supported in part by the National Key R&D Program of China (Grant No. 2018YFA0305800), the Strategic Priority Research Program of the Chinese Academy of Sciences (Grant No. XDB28000000), the National Natural Science Foundation of China (Grant No. 11834014), and Beijing Municipal Science and Technology Commission (Grant No. Z191100007219013). B.G. is also supported by the National Natural Science Foundation of China (Grants No. Y81Z01A1A9 and No. 12074378), the Chinese Academy of Sciences (Grants No. Y929013EA2 and No. E0EG4301X2), the University of Chinese Academy of Sciences (Grant No. 110200M208), the Strategic Priority Research Program of Chinese Academy of Sciences (Grant No. XDB33000000), and the Beijing Natural Science Foundation (Grant No. Z190011). S.M. was supported by JSPS KAKENHI (Grant No. JP20H01865).

-
- [1] D. Kennedy, *Science* **309**, 75 (2005).
 [2] H. Ohno, *Science* **281**, 951 (1998).
 [3] L. Chen, X. Yang, F. Yang, J. Zhao, J. Misuraca, P. Xiong, and S. von Molna, *Nano Lett.* **11**, 2584 (2011).
 [4] T. Dietl, *Nat. Mater.* **9**, 965 (2010).
 [5] J. Mašek, J. Kudrnovsky, F. Maca, B. L. Gallagher, R. P. Campion, D. H. Gregory, and T. Jungwirth, *Phys. Rev. Lett.* **98**, 067202 (2007).
 [6] Z. Deng, C. Jin, Q. Liu, X. Wang, J. Zhu, S. Feng, L. Chen, R. Yu, C. Arguello, T. Goko, F. Ning, J. Zhang, Y. Wang, A. Aczel, T. Munsie, T. Williams, G. Luke, T. Kakeshita, S. Uchida, W. Higemoto, T. Ito, B. Gu, S. Maekawa, G. Morris, and Y. Uemura, *Nat. Commun.* **2**, 422 (2011).
 [7] Z. Deng, K. Zhao, B. Gu, W. Han, J. L. Zhu, X. C. Wang, X. Li, Q. Q. Liu, R. C. Yu, T. Goko, B. Frandsen, L. Liu, J. Zhang, Y. Wang, F. L. Ning, S. Maekawa, Y. J. Uemura, and C. Q. Jin, *Phys. Rev. B* **88**, 081203(R) (2013).
 [8] K. Zhao, Z. Deng, X. C. Wang, W. Han, J. L. Zhu, X. Li, Q. Q. Liu, R. C. Yu, T. Goko, B. Frandsen, L. Liu, F. Ning, Y. J. Uemura, H. Dabkowska, G. M. Luke, H. Luetkens, E. Morenzoni, S. R. Dunsiger, A. Senyshyn, P. Boni, and C. Q. Jin, *Nat. Commun.* **4**, 1442 (2013).
 [9] K. Zhao, B. Chen, G. Zhao, Z. Yuan, Q. Liu, Z. Deng, J. Zhu, and C. Jin, *Chin. Sci. Bull.* **59**, 2524 (2014).
 [10] J. K. Glasbrenner, I. ˘Zutic, and I. I. Mazin, *Phys. Rev. B* **90**, 140403(R) (2014).

- [11] H. Suzuki, K. Zhao, G. Shibata, Y. Takahashi, S. Sakamoto, K. Yoshimatsu, B. J. Chen, H. Kumigashira, F.-H. Chang, H.-J. Lin, D. J. Huang, C. T. Chen, B. Gu, S. Maekawa, Y. J. Uemura, C. Q. Jin, and A. Fujimori, *Phys. Rev. B* **91**, 140401(R) (2015).
- [12] H. Suzuki, G. Q. Zhao, K. Zhao, B. J. Chen, M. Horio, K. Koshiishi, J. Xu, M. Kobayashi, M. Minohara, E. Sakai, K. Horiba, H. Kumigashira, B. Gu, S. Maekawa, Y. J. Uemura, C. Q. Jin, and A. Fujimori, *Phys. Rev. B* **92**, 235120 (2015).
- [13] N. T. Tu, P. N. Hai, L. D. Anh, and M. Tanaka, *Appl. Phys. Lett.* **108**, 192401 (2016).
- [14] S. Goel, L. D. Anh, S. Ohya, and M. Tanaka, *Phys. Rev. B* **99**, 014431 (2019).
- [15] S. Goel, L. D. Anh, N. T. Tu, S. Ohya, and M. Tanaka, *Phys. Rev. Mater.* **3**, 084417 (2019).
- [16] K. Takiguchi, L. D. Anh, T. Chiba, T. Koyama, D. Chiba, and M. Tanaka, *Nat. Phys.* **15**, 1134 (2019).
- [17] B. Gu and S. Maekawa, *Phys. Rev. B* **94**, 155202 (2016).
- [18] B. Gu and S. Maekawa, *AIP Adv.* **7**, 055805 (2016).
- [19] B. Gu, *J. Semicond.* **40**, 081504 (2019).
- [20] A. V. Kudrin, Y. A. Danilov, V. P. Lesnikov, M. V. Dorokhin, O. V. Vikhrova, D. A. Pavlov, Y. V. Usov, I. N. Antonov, R. N. Kriukov, A. V. Alaferdov, and N. A. Sobolev, *J. Appl. Phys.* **122**, 183901 (2017).
- [21] N. T. Tu, P. N. Hai, L. D. Anh, and M. Tanaka, *Appl. Phys. Lett.* **112**, 122409 (2018).
- [22] N. T. Tu, P. N. Hai, L. D. Anh, and M. Tanaka, *Appl. Phys. Express* **12**, 103004 (2019).
- [23] P. Zhang, Y.-H. Kim, and S.-H. Wei, *Phys. Rev. Appl.* **11**, 054058 (2019).
- [24] S. Guo, H. Man, K. Wang, C. Ding, Y. Zhao, L. Fu, Y. Gu, G. Zhi, B. A. Frandsen, S. C. Cheung, Z. Guguchia, K. Yamakawa, B. Chen, H. Wang, Z. Deng, C. Q. Jin, Y. J. Uemura, and F. Ning, *Phys. Rev. B* **99**, 155201 (2019).
- [25] E. Abe, F. Matsukura, H. Yasuda, Y. Ohno, and H. Ohno, *Phys. E* **7**, 981 (2000).
- [26] K. Ganesan and H. L. Bhat, *J. Appl. Phys.* **103**, 043701 (2008).
- [27] P. N. Hai, L. D. Anh, S. Mohan, T. Tamegai, M. Kodzuka, T. Ohkubo, K. Hono, and M. Tanaka, *Appl. Phys. Lett.* **101**, 182403 (2012).
- [28] P. N. Hai, L. D. Anh, and M. Tanaka, *Appl. Phys. Lett.* **101**, 252410 (2012).
- [29] T. Schallenberg and H. Munekata, *Appl. Phys. Lett.* **89**, 042507 (2006).
- [30] M. Yamanouchi, J. Ieda, F. Matsukura, S. E. Barnes, S. Maekawa, and H. Ohno, *Science* **317**, 1726 (2007).
- [31] J. Fabian, I. Žutić, and S. D. Sarma, *Appl. Phys. Lett.* **84**, 85 (2004).
- [32] P. Hohenberg and W. Kohn, *Phys. Rev.* **136**, B864 (1964).
- [33] W. Kohn and L. J. Sham, *Phys. Rev.* **140**, A1133 (1965).
- [34] J. E. Hirsch and R. M. Fye, *Phys. Rev. Lett.* **56**, 2521 (1986).
- [35] B. Gu, N. Bulut, and S. Maekawa, *J. Appl. Phys.* **104**, 103906 (2008).
- [36] J.-ichiro Ohe, Y. Tomoda, N. Bulut, R. Arita, K. Nakamura, and S. Maekawa, *J. Phys. Soc. Jpn.* **78**, 083703 (2009).
- [37] B. Gu, N. Bulut, T. Ziman, and S. Maekawa, *Phys. Rev. B* **79**, 024407 (2009).
- [38] B. Gu, J.-Y. Gan, N. Bulut, T. Ziman, G.-Y. Guo, N. Nagaosa, and S. Maekawa, *Phys. Rev. Lett.* **105**, 086401 (2010).
- [39] B. Gu, I. Sugai, T. Ziman, G. Y. Guo, N. Nagaosa, T. Seki, K. Takanashi, and S. Maekawa, *Phys. Rev. Lett.* **105**, 216401 (2010).
- [40] Z. Xu, B. Gu, M. Mori, T. Ziman, and S. Maekawa, *Phys. Rev. Lett.* **114**, 017202 (2015).
- [41] F. D. M. Haldane and P. W. Anderson, *Phys. Rev. B* **13**, 2553 (1976).
- [42] P. Blaha, K. Schwart, G. K. H. Hadsen, D. Kvasnicka, and J. Luitz, *WIEN2K, An Augmented Plane Wave Plus Local Orbitals Program for Calculating Crystal Properties* (Vienna University of Technology, Vienna, 2001).
- [43] F. Tran and P. Blaha, *Phys. Rev. B* **83**, 235118 (2011).
- [44] N. Bulut, K. Tanikawa, S. Takahashi, and S. Maekawa, *Phys. Rev. B* **76**, 045220 (2007).
- [45] Y. Tomoda, N. Bulut, and S. Maekawa, *Phys. B* **404**, 1159 (2009).
- [46] W. Han, B. J. Chen, B. Gu, G. Q. Zhao, S. Yu, X. C. Wang, Q. Q. Liu, Z. Deng, W. M. Li, J. F. Zhao, L. P. Cao, Y. Peng, X. Shen, X. H. Zhu, R. C. Yu, S. Maekawa, Y. J. Uemura, and C. Q. Jin, *Sci. Rep.* **9**, 7490 (2019).
- [47] E. Litwin-Staszewska, W. Szymańska, and R. Piotrzkowski, *Phys. Status Solidi (b)* **106**, 551 (1981).
- [48] R. K. Willardson and A. C. Beer (eds.), *Semiconductor and Semimetals* (Academic Press, New York, 1977).